Published in final edited form as:
Biochemistry. 2013 December 23; 52(51): 9223–9236. doi:10.1021/bi400987k.

Molecular Origin of the Binding of WWOX Tumor Suppressor to ErbB4 Receptor Tyrosine Kinase

Brett J. Schuchardt[1], **Vikas Bhat**[1], **David C. Mikles**[1], **Caleb B. McDonald**[1], **Marius Sudol**[2,3], and **Amjad Farooq**[1,*]

[1]Department of Biochemistry & Molecular Biology, Leonard Miller School of Medicine, University of Miami, Miami, FL 33136

[2]Weis Center for Research, Geisinger Clinic, Danville, PA 17822

[3]Department of Medicine, Mount Sinai School of Medicine, New York, NY 10029

Abstract

The ability of WWOX tumor suppressor to physically associate with the intracellular domain (ICD) of ErbB4 receptor tyrosine kinase is believed to play a central role in down-regulating the transcriptional function of the latter. Herein, using various biophysical methods, we show that while the WW1 domain of WWOX binds to PPXY motifs located within the ICD of ErbB4 in a physiologically-relevant manner, the WW2 domain does not. Importantly, while the WW1 domain absolutely requires the integrity of the PPXY consensus sequence, non-consensus residues within and flanking this motif do not appear to be critical for binding. This strongly suggests that the WW1 domain of WWOX is rather promiscuous toward its cellular partners. We also provide evidence that the lack of binding of WW2 domain of WWOX to PPXY motifs is due to the replacement of a signature tryptophan, lining the hydrophobic ligand binding groove, with tyrosine (Y85). Consistent with this notion, the Y85W substitution within the WW2 domain exquisitely restores its binding to PPXY motifs in a manner akin to the binding of WW1 domain of WWOX. Of particular significance is the observation that WW2 domain augments the binding of WW1 domain to ErbB4, implying that the former serves as a chaperone within the context of the WW1–WW2 tandem module of WWOX in agreement with our findings reported previously. Taken together, our study sheds new light on the molecular basis of an important WW-ligand interaction involved in mediating a plethora of cellular processes.

Keywords

WW domain-ligand interactions; WW domain engineering; WW tandem module; Molecular modeling; Molecular dynamics

INTRODUCTION

While the role of ErbB4 receptor tyrosine kinase in mediating transmembrane signaling as well as being a prognostic factor in many human diseases is well-documented (1–8), its complex structural architecture continues to surprise us in terms of its ability to modulate downstream cellular activities via novel modes of action. Notably, ErbB4 harbors the canonical ECD-TM-ICD modular cassette, where the central single-helical transmembrane (TM) domain is flanked between an N-terminal extracellular (ECD) and a C-terminal intracellular (ICD) domains (Figure 1a). Upon stimulation with its extracellular ligand

*To whom correspondence should be addressed: amjad@farooqlab.net | tel 305-243-2429 | fax 305-243-3955.

heregulin or in response to TPA-induced activation of protein kinase C, ErbB4 undergoes intracellular proteolytic cleavage by γ-secretase (9, 10). This action releases the ICD and marks the initiation of ErbB4 intracellular signaling in what appears to be a relatively new paradigm of signal transduction (11, 12). In particular, similar mechanisms have also been reported for the proteolytic processing of the Notch receptor and the Alzheimer's amyloid precursor protein (13–15).

Importantly, the ICD of ErbB4 contains putative PPXY motifs (designated PY1, PY2 and PY3) that serve as recognition sites for the recruitment of WW-containing proteins such as YAP transcriptional regulator (16, 17), WWOX tumor suppressor (18), and ITCH ubiquitin ligase (19). The physical association between YAP and ICD facilitates translocation of the latter to the nucleus (16), where it is believed to regulate the transcription of hitherto unidentified target genes involved in key cellular processes including embryonic development (20). It should be noted here that ICD of ErbB4 is a much more potent co-activator of YAP2 than YAP1 (16). While YAP acts as transcriptional co-activator of ErbB4, interaction with WWOX not only results in cytoplasmic sequestration of ICD but also suppresses its transcriptional co-activation by YAP (18). On the other hand, binding to ITCH promotes polyubiquitination and degradation of ErbB4, thereby regulating its stability and the availability of ICD for subsequent transcriptional regulation in the nucleus (19). In this manner, WWOX and ITCH antagonize the co-activation function of YAP by virtue of their ability to bind to the ICD of ErbB4 in a competitive manner. In this study, we focus our efforts on uncovering the molecular basis of WWOX-ErbB4 interaction. The fact that WWOX and ErbB4 are co-expressed in breast cancer renders our study all the more relevant and timely (21).

The WWOX tumor suppressor, comprised of a tandem copy of WW domains (designated WW1 and WW2) located N-terminal to the short-chain dehydrogenase/reductase (SDR) domain (Figure 1b), orchestrates a diverse array of cellular activities, including growth, proliferation, apoptosis and tumor suppression (22–25). In particular, the WWOX gene spans the 16q23 fragile chromosomal region involved in cancer. The fact that the aberrant expression of WWOX tumor suppressor is believed to be linked to the progression of many forms of cancer, including those of breast and prostate (26–33), is telling. Moreover, disruption of WWOX gene in mice results in defective metabolism, impaired growth and post-natal lethality, implying that WWOX serves a non-redundant role that cannot be compensated by other cellular proteins (34–36). This argument is further supported by the fact that WWOX is expressed in several distinct isoforms across various tissues, thereby further complicating its role in cellular signaling networks central to health and disease. In addition to its key role in mediating the transcriptional regulation of ErbB4 (18), WWOX also serves as a transcriptional regulator of a diverse array of other ligands such as p73, RUNX, AP2 and NF-κB transcription factors as well as many other cellular proteins including SIMPLE, Ezrin and WBP1/2 (22, 37–39). Most importantly, the WWOX-ligand interactions are believed to be largely driven by the binding of proline-rich PPXY motifs found within cognate ligands to the WW domains of WWOX in a canonical manner (40–42).

In order to understand the molecular basis of WWOX-ErbB4 interaction, we provide herein a detailed analysis of the binding of WW domains of WWOX to PPXY motifs located within the ICD of ErbB4 using various biophysical methods. Our study shows that while the WW1 domain of WWOX binds to PPXY motifs located within the ICD of ErbB4 in a physiologically-relevant manner, the WW2 domain does not. This notion thereby further corroborates our previous finding that WW2 likely serves as an orphan domain (43). We also provide evidence that the lack of binding of WW2 domain is due to the replacement of a signature tryptophan, that forms a part of the network of residues lining the canonical

hydrophobic binding groove within the triple-stranded β-sheet fold of WW domains, with tyrosine (Y85). Of particular significance is the observation that WW2 domain augments the binding of WW1 domain to ErbB4, implying that the former serves as a chaperone within the context of the WW1–WW2 tandem module of WWOX in agreement with our findings reported previously (43).

MATERIALS and METHODS

Protein preparation

WW1 domain (residues 16–50), WW2 domain (residues 57–91) and WW1–WW2 tandem module (residues 16–91) of human WWOX were cloned into pET30 bacterial expression vectors with an N-terminal His-tag using Novagen LIC technology as described earlier (43). The mutant construct containing the Y85W single substitution within the WW2 domain (WW2W) was generated using the PCR primer extension method (44). All recombinant proteins were subsequently expressed in Escherichia coli BL21*(DE3) bacterial strain (Invitrogen) and purified on a Ni-NTA affinity column using standard procedures as described previously (43). Further treatment on a Hiload Superdex 200 size-exclusion chromatography (SEC) column coupled in-line with GE Akta FPLC system led to purification of recombinant domains to apparent homogeneity as judged by SDS-PAGE analysis. Final yield was typically between 50–100mg protein of apparent homogeneity per liter of bacterial culture. Protein concentration was determined spectrophotometrically on the basis of extinction coefficients calculated for each recombinant construct using the online software ProtParam at ExPasy Server (45).

Peptide synthesis

12-mer wildtype and mutant peptides spanning various PPXY motifs within the ICD of human ErbB4 were commercially obtained from GenScript Corporation. The amino acid sequence of these peptides is shown in Figure 1a. The peptide concentrations were measured gravimetrically.

Isothermal titration calorimetry

Isothermal titration calorimetry (ITC) experiments were performed on a Microcal VP-ITC instrument. All measurements were repeated at least three times. Briefly, WW domains of WWOX alone or in the context of the WW1–WW2 tandem module and ErbB4 peptides were dialyzed in 50mM Sodium phosphate, 100mM NaCl, 1mM EDTA and 5mM β-mercaptoethanol at pH 7.0. All experiments were initiated by injecting 25 × 10μl aliquots of 4 mM of each ErbB4 peptide from the syringe into the calorimetric cell containing 1.46ml of 40–60 μM of WW domains of WWOX alone or in the context of the WW1–WW2 tandem module at 25 °C. The change in thermal power as a function of each injection was automatically recorded using the ORIGIN software and the raw data were further processed to yield binding isotherms of heat release per injection as a function of molar ratio of each peptide to WW domain construct. The heats of mixing and dilution were subtracted from the heat of binding per injection by carrying out a control experiment in which the same buffer in the calorimetric cell was titrated against each peptide in an identical manner. To extract the equilibrium dissociation constant (K_d) and the enthalpic change (ΔH) associated with binding, the ITC isotherms were iteratively fit to a one-site binding model by non-linear least squares regression analysis using the integrated ORIGIN software as described earlier (43, 46). Notably, all binding stoichiometries were fixed to unity while ΔH and K_d were allowed to float during the fitting procedure to improve the accuracy of thermodynamic parameters. The free energy change (ΔG) upon peptide binding was calculated from the relationship:

$$\Delta G = RT \ln K_d \quad [1]$$

where R is the universal molar gas constant (1.99 cal/K/mol) and T is the absolute temperature. The entropic contribution (TΔS) to the free energy of binding was calculated from the relationship:

$$T\Delta S = \Delta H - \Delta G \quad [2]$$

where ΔH and ΔG are as defined above.

Analytical light scattering

Analytical light scattering (ALS) experiments were conducted at 10°C on a Wyatt miniDAWN TREOS triple-angle static light scattering detector and Wyatt QELS dynamic light scattering detector coupled inline with a Wyatt Optilab rEX differential refractive index detector and interfaced to a Hiload Superdex 200 size-exclusion chromatography (SEC) column under the control of a GE Akta FPLC system. Briefly, WW domains of WWOX alone or in the context of the WW1–WW2 tandem module were dialyzed in 50mM Sodium phosphate, 100mM NaCl, 1mM EDTA and 5mM β-mercaptoethanol at pH 7.0. Each protein construct was loaded onto the SEC column at a starting concentration of 100–200μM and at a flow rate of 1ml/min and data were automatically acquired using the ASTRA software. The angular- and concentration-dependence of static light scattering (SLS) intensity of each protein construct resolved in the flow mode was measured by the Wyatt miniDAWN TREOS detector. The SLS data were analyzed according to the following built-in Zimm equation in ASTRA software (47, 48):

$$[Kc/R_\theta] = ((1/M) + 2A_2c)[1 + ((16\pi^2(R_g)^2/3\lambda^2)\sin^2(\theta/2))] \quad [4]$$

where R_θ is the excess Raleigh ratio due to protein in solution as a function of protein concentration c (mg/ml) and the scattering angle θ (42°, 90° and 138°), M is the observed molar mass of each protein species, A_2 is the second virial coefficient, λ is the wavelength of laser light in solution (658nm), R_g is the radius of gyration of protein, and K is given by the following relationship:

$$K = [4\pi^2 n^2 (dn/dc)^2]/N_A\lambda^4 \quad [5]$$

where n is the refractive index of the solvent, dn/dc is the refractive index increment of the protein in solution and N_A is the Avogadro's number ($6.02\times10^{23}mol^{-1}$). Under dilute protein concentrations ($c \rightarrow 0$), Eq [4] reduces to:

$$[Kc/R_\theta] = [1/M + ((16\pi^2(R_g)^2/3M\lambda^2)\sin^2(\theta/2))] \quad [6]$$

Thus, a plot of $[Kc/R_\theta]$ versus $\sin^2(\theta/2)$ yields a straight line with slope $16\pi^2R_g^2/3M\lambda^2$ and y-intercept 1/M. It should be noted here that the scattered light by the WW domains of WWOX alone or in the context of the WW1–WW2 tandem module displayed no observable angular-dependence, thereby rendering the determination of R_g for each construct unpractical. Nonetheless, M was obtained in a global analysis from the y-intercept of linear fits of a series of $[Kc/R_\theta]$-$\sin^2(\theta/2)$ plots as a function of protein concentration along the elution profile of each protein species using SLS measurements at three scattering angles. The weighted-average molar mass (M_w) and number-average molar mass (M_n) were calculated from the following relationships:

$$M_w = \sum(c_i M_i) / \sum c_i \quad [7]$$

$$M_n = \sum c_i / \sum(c_i / M_i) \quad [8]$$

where c_i is the protein concentration and M_i is the observed molar mass at the ith slice within an elution profile. The time- and concentration-dependence of dynamic light scattering (DLS) intensity fluctuation of each protein construct resolved in the flow mode was measured by the Wyatt QELS detector positioned at 90° with respect to the incident laser beam. The DLS data were iteratively fit using nonlinear least squares regression analysis to the following built-in equation in ASTRA software (49–51):

$$G(\tau) = \alpha \mathrm{Exp}(-2\Gamma\tau) + \beta \quad [9]$$

where G(τ) is the autocorrelation function of dynamic light scattering intensity fluctuation I, τ is the delay time of autocorrelation function, Λ is the decay rate constant of autocorrelation function, α is the initial amplitude of autocorrelation function at zero delay time, and β is the baseline offset (the value of autocorrelation function at infinite delay time). Thus, fitting the above equation to a range of G(τ)-τ plots as a function of protein concentration along the elution profile of each protein species was used to compute the weighted-average value of Λ using DLS measurements at a scattering angle of 90°. Next, the translational diffusion coefficient (D_t) of each protein species was calculated from the following relationship:

$$D_t = [(\Gamma\lambda^2) / (16\pi^2 n^2 \sin^2(\theta/2))] \quad [10]$$

where λ is the wavelength of laser light in solution (658nm), n is the refractive index of the solvent and θ is the scattering angle (90°). Additionally, the hydrodynamic radius (R_h) of each protein construct was determined from the Stokes-Einstein relationship:

$$R_h = [(k_B T) / (6\pi\eta D_t)] \quad [11]$$

where k_B is Boltzman's constant ($1.38\times10^{-23} JK^{-1}$), T is the absolute temperature and η is the solvent viscosity. Notably, the R_h reported here represents the weighted-average value as defined by the following expression:

$$R_h = \sum(c_i R_{h,i}) / \sum c_i \quad [12]$$

where c_i is the protein concentration and $R_{h,i}$ is the observed hydrodynamic radius at the ith slice within an elution profile. It is also noteworthy that, in both the SLS and DLS measurements, protein concentration (c) along the elution profile of each protein species was automatically quantified in the ASTRA software from the change in refractive index (Δn) with respect to the solvent as measured by the Wyatt Optilab rEX detector using the following relationship:

$$c = (\Delta n) / (dn/dc) \quad [13]$$

where dn/dc is the refractive index increment of the protein in solution.

Molecular modeling

Molecular modeling (MM) was employed to build atomic structures of WW1 and WW2 domains of WWOX in the context of a tandem module and individually in complex with a peptide containing the PY3 motif located within the ICD of ErbB4 (ErbB4_PY3) using the

MODELLER software based on homology modeling (52). For individual liganded WW domains, the NMR structure of the homologous WW domain of YAP bound to a peptide containing the PPXY motif was used as a template (PDBID 1JMQ). For the unliganded tandem WW1–WW2 module, the NMR structure of the tandem WW1–WW2 module of FBP21 was used as a template (PDBID 2JXW). A total of 100 atomic models were calculated and the structure with the lowest energy, as judged by the MODELLER Objective Function, was selected for further analysis. The atomic models were rendered using RIBBONS (53).

Molecular dynamics

Molecular dynamics (MD) simulations were performed with the GROMACS software (54) using the integrated AMBER99SB-ILDN force field (55). Briefly, the structural models of WW1 and WW2 domains of WWOX in the context of a tandem module and individually in complex with ErbB4_PY3 peptide were each centered in a cubic box with dimensions of 10Å and hydrated using the extended simple point charge (SPC/E) water model (56). The ionic strength of solution was set to 100mM with NaCl and the hydrated structures were energy-minimized with the steepest descent algorithm prior to equilibration under the NPT ensemble conditions, wherein the number of atoms (N), pressure (P) and temperature (T) within the system were kept constant. The Particle-Mesh Ewald (PME) method (57) was employed to compute long-range electrostatic interactions with a spherical cut-off of 10Å and a grid space of 1.6Å with a fourth order interpolation. The Linear Constraint Solver (LINCS) algorithm was used to restrain bond lengths (58). All MD simulations were performed under periodic boundary conditions (PBC) at 300K using the leap-frog integrator with a time step of 2fs. For the final MD production runs, data were collected every ns over a time scale of 250ns. Structural snapshots taken at various intervals during the course of MD simulations were rendered using RIBBONS (53).

RESULTS and DISCUSSION

WW1 domain of WWOX binds to PPXY motifs in ErbB4 with distinct affinities

To uncover the molecular basis of WWOX-ErbB4 interaction, we measured the binding of WW domains of WWOX to PPXY peptides derived from potential WWOX-binding sites in ErbB4 using ITC. While representative ITC isotherms for the binding of WW1 domain are shown in Figure 2, no binding was observed for the WW2 domain to any of the PPXY motif even when external conditions including temperature, ionic strength and pH were altered. This salient observation strongly argues that WW2 domain of WWOX does not harbor intrinsic potential to interact with PPXY motifs derived from ErbB4, thereby further corroborating our previous finding that WW2 likely serves as an orphan domain (43). On the other hand, the WW1 domain binds to all three PPXY motifs located within ErbB4 but in a distinct manner (Table 1). Thus, while binding of WW1 domain to ErbB4_PY3 motif occurs with an affinity a little over 100μM, it recognizes the ErbB4_PY1 and ErbB4_PY2 motifs in the order of hundreds of micromolar. Despite these differences, binding of WW1 domain of WWOX to all three PPXY motifs is predominantly driven by favorable enthalpic forces accompanied by small unfavorable or favorable entropic changes. Notably, the enthalpically-driven nature of the WW-PPXY interaction suggests the formation of specific intermolecular interactions such as hydrogen bonding and van der Waals contacts that likely underscore the fidelity of this key protein-protein interaction. In contrast, the overall unfavorable entropic changes most likely result from the loss of degrees of freedom available to both partners upon intermolecular association.

In order to understand the molecular factors that drive the binding of WW1 domain of WWOX to various PPXY motifs in ErbB4 with differential affinities (Table 1), we next

performed alanine scan on the ErbB4_PY3 peptide and measured the binding of each mutant peptide to WW1 domain as described above (Table 2). Strikingly, our data reveal that alanine substitution of non-consensus residues within and flanking the PPXY motif within the ErbB4_PY3 peptide has little or negligible effect on the binding of WW1 domain. This finding suggests that non-consensus residues within and flanking the PPXY motifs are not critical for driving the WWOX-ErbB4 interaction but they may be important for stabilizing the conformation of PPXY peptides. It is however noteworthy that the alanine substitution of P+2 and R+4 residues—according to the nomenclature presented in Figure 1a—within the ErbB4_PY3 peptide slightly mitigates the binding of WW1 domain. This implies that the presence of a proline and a charged/bulky residue respectively at the +2 and +4 positions may account for the binding of ErbB4_PY3 peptide to WW1 domain with higher affinity relative to the other two peptides. Indeed, the P+2 and R+4 residues within ErbB4_PY3 peptide are respectively replaced by non-proline and non-charged/non-bulky residues at the structurally-equivalent positions in ErbB4_PY1 and ErbB4_PY2 peptides. In particular, the importance of a proline at the +2 position may be accounted for by the virtue of its ability to buttress the polyproline II (PPII) helical conformation of ErbB4_PY3 peptide required for its optimal binding to the WW1 domain (59–62). Taken together, our thermodynamic analysis shows that the WW1 domain of WWOX binds to ErbB4 peptides in a rather promiscuous fashion with a subtle contribution of non-consensus residues within and flanking the PPXY motifs to the overall free energy of binding.

Structural analysis provides physical basis for the binding of WW1 domain and lack thereof of WW2 domain of WWOX to PPXY motifs within ErbB4

To understand the physical basis of the binding of WW1 domain and lack thereof of WW2 domain of WWOX to PPXY motifs within ErbB4, we built their respective structural models in complex with the ErbB4_PY3 peptide (Figure 3). Our structural analysis reveals that the ErbB4_PY3 peptide adopts the PPII-helical conformation and binds within the hydrophobic groove of the triple-stranded β-sheet fold of WW1 domain in a canonical manner (59–62) (Figure 3a). Consistent with our thermodynamic data presented above (Tables 1 and 2), the consensus residues within the PPXY motif appear to be exclusively engaged in key intermolecular contacts with specific residues lining the hydrophobic groove of WW1 domain, while non-consensus residues within and flanking the PPXY motif make no discernable intermolecular contacts. Briefly, the pyrrolidine moiety of P0, the first proline within the PPXY motif according to the nomenclature presented in Figure 1a, stacks against the indole sidechain of W44 in WW1 domain (Figure 3a). It should be noted here that W44 represents one of the two signature tryptophan residues that lend their name to WW domains. On the other hand, the sidechain moieties of Y33/T42 residues within the WW1 domain sandwich the pyrrolidine ring of P+1 within the PPXY motif. Finally, the phenyl moiety of Y+3, the terminal tyrosine within the PPXY motif, buries deep into the hydrophobic groove and is escorted by sidechain atoms of the A35/H37/E40 triad in WW1 domain.

It is telling that the various interactions between specific sidechain groups in the WW1 domain and the ErbB4_PY3 peptide are stabilized by an extensive network of van der Waals contacts and hydrogen bonding (Figure 3a). Importantly, the Hη phenolic hydrogen of Y+3 residue appears to hydrogen bond with the Nδ1 imidazole nitrogen of H37 in WW1 domain. On the other hand, the E40 residue in WW1 domain stabilizes the aromatic ring of Y+3 within the ErbB4_PY3 peptide by virtue of the apolar character of its -CγH2- methylene atoms while its negatively charged carboxyl group points away to avoid unfavorable contact with Y+3. Of particular note is the observation that the pyrrolidine ring of P+2 within the ErbB4_PY3 peptide in complex with WW1 domain is fully solvent-exposed (not shown). This strongly argues that the P+2 residue, which is replaced by a non-proline in ErbB4_PY1

and ErbB4_PY2 peptides, may play an important role in the stabilization of PPII-helical conformation of ErbB4_PY3 peptide. Accordingly, the presence of a proline at the +2 position could account for the binding of ErbB4_PY3 peptide to WW1 domain with higher affinity relative to the other two peptides, as suggested by our thermodynamic data (Tables 1 and 2), by virtue of its ability to lower the entropic penalty to the overall free energy of binding.

Equally importantly, while our alanine scan suggests that none of the residues flanking the PPXY motif are critical for binding to WW1 domain in terms of the change in overall free energy (ΔG), the underlying changes in enthalpic contribution (ΔH) nonetheless paint a very different picture (Table 2). In particular, the enthalpic change associated with the binding of mutant PY3_A+5 peptide, harboring an alanine in place of H+5, is concomitant with the release of more than −5 kcal/mol of favorable enthalpy relative to the PY3_WT peptide. While we note the difficulties associated with accurate determination of ΔH associated with weak macromolecular interactions, it is nevertheless conceivable that the much less bulkier size of alanine enables the PY3_A+5 mutant peptide to engage in closer intermolecular contacts with the WW1 domain relative to PY3_WT peptide. However, the resulting release of more favorable enthalpy appears to be offset and largely compensated by an equal but unfavorable change in entropy in agreement with the ubiquitous enthalpy-entropy compensation phenomenon that governs macromolecular interactions (Table 2). It is also noteworthy that water-mediated hydrogen bonding has been recently shown to play a key role in driving the binding of proline-rich ligands to SH3 domains (63–65). Thus, although the role of water in mediating WW-ligand interactions has not been directly probed, it is possible that hydration also plays an important role in fine tuning the affinity of various ErbB4 peptides to the WW1 domain of WWOX in addition to the role of specific intermolecular interactions.

More importantly, our structural analysis provides a tantalizing rationale for the lack of binding of WW2 domain of WWOX to ErbB4 peptides (Figure 3b). The fact that all residues but W44 in WW1 domain involved in intermolecular contacts with ErbB4_PY3 peptide are highly conserved within the hydrophobic groove of the WW2 domain is striking. Thus, the Y33/T42 pair in WW1 domain that serves as a counterpart for accommodating P +1 is substituted by a relatively conservative F74/T83 pair in WW2 domain. In a similar manner, the A35/H37/E40 triad in WW1 domain that escorts Y+3 is replaced by a relatively conserved V76/H78/K81 triad in WW2 domain. However, W44 residue in WW1 domain—whose indole sidechain is involved in the stabilization of P0—is replaced by Y85 in WW2 domain. Given the distinguishing chemistry and apolar character of the aromatic rings of W44 and Y85, we reason that this tryptophan-tyrosine substitution within the WW2 domain most likely accounts for its lack of binding to PPXY motifs. To test the validity of this hypothesis, we introduced the Y85W substitution within the WW2 domain and subsequently measured the binding of this mutant WW2 domain, hereinafter referred to as WW2W domain, to various ErbB4 peptides using ITC (Table 3). Our data indicate that while WW2W mutant domain recognizes ErbB4_PY1 and ErbB4_PY2 peptides rather weakly, it binds to the ErbB4_PY3 peptide with an affinity that is more than two-fold stronger than that observed for the binding of WW1 domain (Tables 1 and 3). Taken together, these findings have an important implication on the engineering of WW domains of WWOX for therapeutic intervention.

WW2 domain augments the binding of WW1 domain in the context of WW1–WW2 tandem module of WWOX to PPXY motifs within ErbB4

We previously reported that while WW1 domain of WWOX is structurally disordered and folds upon ligand binding (43), the WW2 domain not only adopts a fully structured conformation but also aids stabilization and ligand binding to WW1 domain. On the basis of

this earlier finding, we postulate that the WW2 domain likely serves as a chaperone to augment the physiological function of WW1 domain within WWOX. To test this hypothesis further, we next conducted ITC analysis on the binding of WW1–WW2 tandem module of WWOX to various ErbB4 peptides (Figure 4). Conspicuously, our data show that the WW1 domain in the context of WW1–WW2 tandem module binds to ErbB4 peptides with affinities that are more than two-fold stronger than those observed for the binding of WW1 domain alone (Tables 1 and 4).

WW domains may lie in close proximity of each other within the WW1–WW2 tandem module of WWOX

Our data presented above, and those reported earlier (43), strongly establish the role of WW2 domain of WWOX as a chaperone in its ability to modulate ligand binding to WW1 domain. The physical basis of how WW2 domain mediates such an allosteric effect however warrants further investigation. Thus, for example, it is conceivable that the WW2 domain physically associates with the WW1 domain and, in so doing, aids its folding. This notion gains further credibility in light of the rather short linker (less than 20 residues) separating the tandem WW domains. On the other hand, it is also conceivable that the WW1–WW2 tandem module adopts a co-linear “dumbbell-like” conformation. Finally, the possibility that the WW1–WW2 tandem module self-associates into a dimer or an higher-order oligomer to adopt quaternary structure cannot be ruled out either. This latter view is supported by the observation that the WW2 domain of SAV1 adaptor, which shares high sequence homology with the WW2 domain of WWOX and has no known ligand, self-associates into a homodimer (66).

In an effort to shed light on the physical basis of how WW2 domain modulates ligand binding to WW1 domain, we next performed ALS analysis on WW domains of WWOX alone and in the context of WW1–WW2 tandem module (Figure 5). Importantly, we also quantified various physical parameters accompanying the solution behavior of WW domains from the first principles of hydrodynamics without any assumptions (Table 5). Our data indicate that WW domains alone and in the context of WW1–WW2 tandem module predominantly adopt a monomeric conformation in solution. This is evidenced by the fact that the observed molar mass for all species in solution is in remarkable agreement with their corresponding molar mass calculated from their amino acid sequence alone (Table 5). Notably, the WW1 domain also harbors some propensity to homodimerize, as indicated by a small left hand shoulder in the corresponding elution profile (Figure 5a). However, the homodimer-monomer equilibrium appears to be largely in favor of the latter species. Given that the ALS analysis was conducted under high protein concentrations (100–200μM)—a practical necessity due to the rather low sensitivity of light scattering detectors—we believe that the propensity of WW1 domain to homodimerize is unlikely to be physiologically relevant. Most importantly, the lack of angular-dependence of static light scattering is indicative of the fact that WW domains alone or in the context of WW1–WW2 tandem module do not self-associate into higher-order oligomers (Figure 5b). This notion is further vindicated by the fact that the M_w/M_n ratio is close to unity for all species (Table 5), implying that the WW domains alone and in the context of WW1–WW2 tandem module are highly monodisperse.

In order to gain insights into macromolecular conformation, we also calculated the hydrodynamic radius (R_h) for each species on the basis of dynamic light scattering (Figure 5c and Table 5). Such analysis reveals that while both WW domains alone display hydrodynamic radius of around 20Å, it only slightly increases in the case of WW1–WW2 tandem module. While this is indicative of the fact that the WW domains may lie in close proximity within the WW1–WW2 tandem module, the alternative possibility that they may also physically associate with each other cannot be excluded either. In order to test this

plausible scenario, we conducted ITC analysis on the binding of WW1 domain of WWOX to WW2 domain and vice versa. Interestingly, our analysis revealed no observable binding between the two WW domains. However, this does not necessarily preclude their physical association in the context of a tandem module, wherein they are physically connected by a short linker. For example, the presence of an interdomain linker is likely to significantly lower the entropic penalty associated with their physical association.

WW1–WW2 tandem module of WWOX displays dynamic plasticity

To further test the extent to which WW domains of WWOX may physically associate with each other, we next conducted MD simulations on the WW1–WW2 tandem module (Figure 6). Briefly, the starting MD conformation of the WW1–WW2 tandem module of WWOX was structurally modeled on the basis of its homology with the tandem WW1–WW2 module of FBP21 pre-mRNA splicing factor (67). As shown in Figure 6a, the MD trajectory reveals that the WW1–WW2 tandem module undergoes a rapid “burst” phase over the first 50ns and then slowly reaches structural equilibrium with a root mean square deviation (RMSD) for the backbone atoms in the neighborhood of 10Å. This rather large value of RMSD is strongly indicative of the fact that the WW domains are unlikely to be physically associated with each other and most probably experience large degrees of freedom relative to each other.

To further glean into the origin of such relative flexibility, we also analyzed the root mean square fluctuation (RMSF) of backbone atoms over the course of MD simulation (Figure 6b). Remarkably, our RMSF analysis reveals that the overall lack of stability of WW1–WW2 tandem module arises from the rather high fluctuations within each of the two constituent WW domains in lieu of the interdomain linker. Notably, the WW1 domain appears to be somewhat less stable compared to WW2 domain, which is in agreement with our observation that the latter serves a chaperonin role for the former. In other words, the relative flexibility of WW1 domain is likely to be important for its ligand binding function, while the relative stability of WW2 domain is a manifestation of its ability to aid the function of WW1 domain. Strikingly, the rather low fluctuations of atoms observed within the interdomain linker with respect to their counterparts within the constituent WW domains implies that their motions may be somewhat restricted relative to each other. This notion is indeed further supported through the assessment of radius of gyration (R_g) of WW1–WW2 tandem module as a function of simulation time (Figure 6c). It is evident from such analysis that the WW1–WW2 tandem module boasts a rather compact conformation, which undergoes rapid expansion as monitored by an increase in R_g during the first 50-ns burst phase. This is followed by a relaxation event that results in the WW1–WW2 tandem module becoming somewhat more compact in size than the starting conformation.

To investigate how a sharp increase followed by a rather slow reduction in R_g relates to conformational changes within the WW1–WW2 tandem module, we took structural snapshots of the protein at various time points during the course of our MD simulation (Figure 7). Consistent with our R_g analysis (Figure 6c), the constituent WW domains within the WW1–WW2 tandem module rapidly fall apart from their close proximity observed in the starting conformation by virtue of the ability of the interdomain linker to uncoil. This relaxation step is slowly followed by compaction in which the two WW domains come together in a manner akin to physical association of two bodies. However, in light of the rather large RMSD observed for the WW1–WW2 tandem domain at structural equilibrium (Figure 6a), it is unlikely that such compact conformation is stable and does not support their physical association so as to adopt a globular fold instead of a dumbbell-like conformation. Nonetheless, while our data presented above cannot ascertain the presence or lack thereof of a stable physical association between the tandem WW domains of WWOX, their remarkable dynamic plasticity could in principle drive their transient physical

association so as to enable the WW2 domain to chaperone the biological function of WW1 domain.

CONCLUSIONS

Receptor tyrosine kinases (RTKs) play a key role in relaying extracellular signals in the form of growth factors, hormones and cytokines to downstream effectors on the cytoplasmic side (68–74). This information is then ultimately integrated via specific signaling cascades to regulate the transcriptional machinery within the nucleus in a wide variety of cellular processes central to human health and disease (75–78). However, in recent years, it has increasingly become clear that RTKs such as ErbB4 may also employ an alternative mechanism to directly affect gene transcription within the nucleus (9, 10, 16). In this new paradigm of signal transduction (11, 12), the RTKs undergo proteolytic processing in response to mitogenic stimulation such that the cleaved fragment on the cytoplasmic side translocates to the nucleus and directly acts as a transcriptional regulator by virtue of its ability to collaborate with other cellular partners such as WWOX.

In an effort to understand the molecular basis of how such cleaved fragments affect gene transcription, we undertook the present work. Toward this goal, our study shows that while WW1 domain of WWOX binds to all three PPXY motifs (PY1–PY3) located within the ICD of ErbB4 in a highly promiscuous manner, the WW2 domain displays no ligand binding potential. Given that we have relied here on short peptides to mimic PPXY motifs in ICD, caution is warranted in that these motifs may depart from their physiological behavior when treated as short peptides due to the loss of local conformational constraints that they may be subject to in the context of ICD. Additionally, the peptides used in our study were purposefully designed with charged amino and carboxyl termini in order to enhance their solubility in an aqueous buffer. While we recognize the fact that the protection of charged termini with amide and acetyl groups would have constituted better models of PPXY motifs, the loss of significant solubility of protected peptides clearly posed more technical challenges. We also note that the physiological relevance of PY1 and PY2 motifs in recruiting WWOX is questionable in light of the rather weak affinity with which they bind to the WW1 domain of WWOX compared to PY3 motif. Interestingly, in vivo studies suggest that the interaction of WWOX with CYT1 and CYT2 isoforms of ErbB4 is indistinguishable (18, 21). Given that CYT1 contains all three PPXY motifs (PY1–PY3) while CYT2 harbors only PY1 and PY3, the role of PY2 motif does not appear to be important for driving the WWOX-ErbB4 interaction. On the other hand, while the binding of YAP to PY3 motif has been demonstrated in vivo, binding to PY1 motif was not observed (16). We also note that Nedd4 ligases such as ITCH, WWP1 and NEDD4 have been suggested to exclusively bind to CYT1 but not CYT2 isoform of ErbB4 (19, 79–82). This finding thus invokes a unique role of PY2 motif in driving the interaction of ErbB4 with Nedd4 members.

On the basis of data presented here, and together with our previous work (43), it appears increasingly likely that the WW2 domain is a putative orphan WW domain that is devoid of ligand binding capability and has evolved as a chaperone to augment the physiological function of WW1 domain within WWOX. This notion is further corroborated by the observation that WWOX binds to its cellular partners exclusively through WW1 domain (18, 22, 37–39). Most importantly, we have also shown here that the ability of WW2 domain to chaperone WW1 domain within WWOX most likely lies in their dynamic plasticity so as to enable the WW2 domain to at least transiently associate with WW1. This scenario would be similar to the tandem WW domains of FBP21 pre-mRNA splicing factor (67) and the fruit fly suppressor of deltex Su(dx) involved in Notch signaling (83). In both of these cases, the tandem WW domains are connected by a highly flexible loop so as to allow them to

move freely with respect to each other without a fixed orientation. On the other hand, stable physical association between the tandem WW domains of WWOX would likely impart rigidity and a fixed orientation upon them in a manner akin to that observed for the tandem WW domains of the yeast splicing factor Prp40 (84). Notably, the interdomain linker in Prp40 is comprised of a well-ordered helix that appears to impart strict rigidity and a fixed orientation upon tandem WW domains. Accordingly, the tandem WW domains in Prp40 essentially act as a single rigid body and the ligand binding grooves lie on opposite faces so as to enable them to bind to distinct ligands and bridge precisely between target sites within the splicing machinery.

It is well-documented that the WW domains can be used to regulate cellular signaling pathways (85, 86). Toward this goal, our demonstration that the WW2 domain of WWOX can be genetically manipulated through Y85W substitution to generate the WW2W engineered domain that recognizes cognate ligands of WW1 domain with high affinity bears therapeutic significance. In particular, the WW1–WW2W engineered tandem module could be therapeutically exploited to negatively regulate signaling pathways in response to hyperactivation of ErbB4 observed in a myriad of human disorders (1–8). In short, our study not only offers molecular insights into the physical and thermodynamic forces at play in the operation of a key WW-ligand interaction involved in mediating a plethora of cellular processes but also new directions on the rationale design of novel therapies harboring greater efficacy coupled with low toxicity for the treatment of human disease.

Acknowledgments

This work was supported by the National Institutes of Health Grant R01-GM083897 and funds from the USylvester Braman Family Breast Cancer Institute (to AF), and by Breast Cancer Coalition grants (RFA #50709 & RFA #60707) from the Department of Health of Pennsylvania (to MS). CBM is a recipient of a postdoctoral fellowship from the National Institutes of Health (Award# T32-CA119929).

ABBREVIATIONS

ALS	Analytical light scattering
CD	Circular dichroism
DLS	Dynamic light scattering
ErbB4	Erythroblastic (Erb) leukemia viral oncogene homolog B4
FBP21	Formin-binding protein 21
ITC	Isothermal titration calorimetry
ITCH	Ubiquitin ligase itchy homolog
LIC	Ligation-independent cloning
MM	Molecular modeling
PPII	Polyproline type II (helix)
RTK	Receptor tyrosine kinase
SEC	Size-exclusion chromatography
SH3	Src homology 3
SLS	Static light scattering
TPA	12-*O*-tetradecanoylphorbol-13-acetate

YAP	YES-associated protein
WWOX	WW domain-containing oxidoreductase

References

1. Sundvall M, Iljin K, Kilpinen S, Sara H, Kallioniemi OP, Elenius K. Role of ErbB4 in breast cancer. J Mammary Gland Biol Neoplasia. 2008; 13:259–268. [PubMed: 18454307]
2. Sundvall M, Veikkolainen V, Kurppa K, Salah Z, Tvorogov D, van Zoelen EJ, Aqeilan R, Elenius K. Cell death or survival promoted by alternative isoforms of ErbB4. Mol Biol Cell. 2010; 21:4275–4286. [PubMed: 20943952]
3. Veikkolainen V, Vaparanta K, Halkilahti K, Iljin K, Sundvall M, Elenius K. Function of ERBB4 is determined by alternative splicing. Cell Cycle. 2011; 10:2647–2657. [PubMed: 21811097]
4. Hollmen M, Liu P, Kurppa K, Wildiers H, Reinvall I, Vandorpe T, Smeets A, Deraedt K, Vahlberg T, Joensuu H, Leahy DJ, Schoffski P, Elenius K. Proteolytic processing of ErbB4 in breast cancer. PLoS One. 2012; 7:e39413. [PubMed: 22761786]
5. Paatero I, Lassus H, Junttila TT, Kaskinen M, Butzow R, Elenius K. CYT-1 isoform of ErbB4 is an independent prognostic factor in serous ovarian cancer and selectively promotes ovarian cancer cell growth in vitro. Gynecol Oncol. 2013; 129:179–187. [PubMed: 23313737]
6. Roskoski R Jr. The ErbB/HER receptor protein-tyrosine kinases and cancer. Biochem Biophys Res Commun. 2004; 319:1–11. [PubMed: 15158434]
7. Burgess AW. EGFR family: structure physiology signalling and therapeutic targets. Growth Factors. 2008; 26:263–274. [PubMed: 18800267]
8. Wadugu B, Kuhn B. The role of neuregulin/ErbB2/ErbB4 signaling in the heart with special focus on effects on cardiomyocyte proliferation. Am J Physiol Heart Circ Physiol. 2012; 302:H2139–2147. [PubMed: 22427524]
9. Ni CY, Murphy MP, Golde TE, Carpenter G. gamma-Secretase cleavage and nuclear localization of ErbB-4 receptor tyrosine kinase. Science. 2001; 294:2179–2181. [PubMed: 11679632]
10. Lee HJ, Jung KM, Huang YZ, Bennett LB, Lee JS, Mei L, Kim TW. Presenilin-dependent gamma-secretase-like intramembrane cleavage of ErbB4. J Biol Chem. 2002; 277:6318–6323. [PubMed: 11741961]
11. Heldin CH, Ericsson J. Signal transduction. RIPping tyrosine kinase receptors apart. Science. 2001; 294:2111–2113. [PubMed: 11739942]
12. Ebinu JO, Yankner BA. A RIP tide in neuronal signal transduction. Neuron. 2002; 34:499–502. [PubMed: 12062033]
13. Artavanis-Tsakonas S, Rand MD, Lake RJ. Notch signaling: cell fate control and signal integration in development. Science. 1999; 284:770–776. [PubMed: 10221902]
14. Fortini ME. Gamma-secretase-mediated proteolysis in cell-surface-receptor signalling. Nat Rev Mol Cell Biol. 2002; 3:673–684. [PubMed: 12209127]
15. Cao X, Sudhof TC. A transcriptionally active complex of APP with Fe65 and histone acetyltransferase Tip60. Science. 2001; 293:115–120. [PubMed: 11441186]
16. Komuro A, Nagai M, Navin NE, Sudol M. WW domain-containing protein YAP associates with ErbB-4 and acts as a co-transcriptional activator for the carboxyl-terminal fragment of ErbB-4 that translocates to the nucleus. J Biol Chem. 2003; 278:33334–33341. [PubMed: 12807903]
17. Omerovic J, Puggioni EM, Napoletano S, Visco V, Fraioli R, Frati L, Gulino A, Alimandi M. Ligand-regulated association of ErbB-4 to the transcriptional co-activator YAP65 controls transcription at the nuclear level. Exp Cell Res. 2004; 294:469–479. [PubMed: 15023535]
18. Aqeilan RI, Donati V, Palamarchuk A, Trapasso F, Kaou M, Pekarsky Y, Sudol M, Croce CM. WW domain-containing proteins, WWOX and YAP, compete for interaction with ErbB-4 and modulate its transcriptional function. Cancer Res. 2005; 65:6764–6772. [PubMed: 16061658]
19. Omerovic J, Santangelo L, Puggioni EM, Marrocco J, Dall'Armi C, Palumbo C, Belleudi F, Di Marcotullio L, Frati L, Torrisi MR, Cesareni G, Gulino A, Alimandi M. The E3 ligase Aip4/Itch

ubiquitinates and targets ErbB-4 for degradation. FASEB J. 2007; 21:2849–2862. [PubMed: 17463226]

20. Hoeing K, Zscheppang K, Mujahid S, Murray S, Volpe MV, Dammann CE, Nielsen HC. Presenilin-1 processing of ErbB4 in fetal type II cells is necessary for control of fetal lung maturation. Biochim Biophys Acta. 2011; 1813:480–491. [PubMed: 21195117]
21. Aqeilan RI, Donati V, Gaudio E, Nicoloso MS, Sundvall M, Korhonen A, Lundin J, Isola J, Sudol M, Joensuu H, Croce CM, Elenius K. Association of Wwox with ErbB4 in breast cancer. Cancer Res. 2007; 67:9330–9336. [PubMed: 17909041]
22. Del Mare S, Salah Z, Aqeilan RI. WWOX: its genomics, partners, and functions. J Cell Biochem. 2009; 108:737–745. [PubMed: 19708029]
23. Bednarek AK, Laflin KJ, Daniel RL, Liao Q, Hawkins KA, Aldaz CM. WWOX, a novel WW domain-containing protein mapping to human chromosome 16q23.3–24.1, a region frequently affected in breast cancer. Cancer Res. 2000; 60:2140–2145. [PubMed: 10786676]
24. Bednarek AK, Keck-Waggoner CL, Daniel RL, Laflin KJ, Bergsagel PL, Kiguchi K, Brenner AJ, Aldaz CM. WWOX, the FRA16D gene, behaves as a suppressor of tumor growth. Cancer Res. 2001; 61:8068–8073. [PubMed: 11719429]
25. Hezova R, Ehrmann J, Kolar Z. WWOX, a new potential tumor suppressor gene. Biomed Pap Med Fac Univ Palacky Olomouc Czech Repub. 2007; 151:11–15. [PubMed: 17690733]
26. Nunez MI, Ludes-Meyers J, Abba MC, Kil H, Abbey NW, Page RE, Sahin A, Klein-Szanto AJ, Aldaz CM. Frequent loss of WWOX expression in breast cancer: correlation with estrogen receptor status. Breast Cancer Res Treat. 2005; 89:99–105. [PubMed: 15692750]
27. Aqeilan RI, Kuroki T, Pekarsky Y, Albagha O, Trapasso F, Baffa R, Huebner K, Edmonds P, Croce CM. Loss of WWOX expression in gastric carcinoma. Clin Cancer Res. 2004; 10:3053–3058. [PubMed: 15131042]
28. Aqeilan RI, Croce CM. WWOX in biological control and tumorigenesis. J Cell Physiol. 2007; 212:307–310. [PubMed: 17458891]
29. Aqeilan RI, Hagan JP, Aqeilan HA, Pichiorri F, Fong LY, Croce CM. Inactivation of the Wwox gene accelerates forestomach tumor progression in vivo. Cancer Res. 2007; 67:5606–5610. [PubMed: 17575124]
30. Pluciennik E, Kusinska R, Potemski P, Kubiak R, Kordek R, Bednarek AK. WWOX--the FRA16D cancer gene: expression correlation with breast cancer progression and prognosis. Eur J Surg Oncol. 2006; 32:153–157. [PubMed: 16360296]
31. Lewandowska U, Zelazowski M, Seta K, Byczewska M, Pluciennik E, Bednarek AK. WWOX, the tumour suppressor gene affected in multiple cancers. J Physiol Pharmacol. 2009; 60(Suppl 1):47–56. [PubMed: 19609013]
32. Zelazowski MJ, Pluciennik E, Pasz-Walczak G, Potemski P, Kordek R, Bednarek AK. WWOX expression in colorectal cancer--a real-time quantitative RT-PCR study. Tumour Biol. 2011; 32:551–560. [PubMed: 21347750]
33. Sudol M, Hunter T. NeW wrinkles for an old domain. Cell. 2000; 103:1001–1004. [PubMed: 11163176]
34. Aqeilan RI, Trapasso F, Hussain S, Costinean S, Marshall D, Pekarsky Y, Hagan JP, Zanesi N, Kaou M, Stein GS, Lian JB, Croce CM. Targeted deletion of Wwox reveals a tumor suppressor function. Proc Natl Acad Sci U S A. 2007; 104:3949–3954. [PubMed: 17360458]
35. Aqeilan RI, Hassan MQ, de Bruin A, Hagan JP, Volinia S, Palumbo T, Hussain S, Lee SH, Gaur T, Stein GS, Lian JB, Croce CM. The WWOX tumor suppressor is essential for postnatal survival and normal bone metabolism. J Biol Chem. 2008; 283:21629–21639. [PubMed: 18487609]
36. Aqeilan RI, Hagan JP, de Bruin A, Rawahneh M, Salah Z, Gaudio E, Siddiqui H, Volinia S, Alder H, Lian JB, Stein GS, Croce CM. Targeted ablation of the WW domain-containing oxidoreductase tumor suppressor leads to impaired steroidogenesis. Endocrinology. 2009; 150:1530–1535. [PubMed: 18974271]
37. Aqeilan RI, Palamarchuk A, Weigel RJ, Herrero JJ, Pekarsky Y, Croce CM. Physical and functional interactions between the Wwox tumor suppressor protein and the AP-2gamma transcription factor. Cancer Res. 2004; 64:8256–8261. [PubMed: 15548692]

38. Aqeilan RI, Pekarsky Y, Herrero JJ, Palamarchuk A, Letofsky J, Druck T, Trapasso F, Han SY, Melino G, Huebner K, Croce CM. Functional association between Wwox tumor suppressor protein and p73, a p53 homolog. Proc Natl Acad Sci U S A. 2004; 101:4401–4406. [PubMed: 15070730]
39. Ludes-Meyers JH, Kil H, Bednarek AK, Drake J, Bedford MT, Aldaz CM. WWOX binds the specific proline-rich ligand PPXY: identification of candidate interacting proteins. Oncogene. 2004; 23:5049–5055. [PubMed: 15064722]
40. Einbond A, Sudol M. Towards prediction of cognate complexes between the WW domain and proline-rich ligands. FEBS Lett. 1996; 384:1–8. [PubMed: 8797792]
41. Sudol M. Structure and function of the WW domain. Prog Biophys Mol Biol. 1996; 65:113–132. [PubMed: 9029943]
42. Sudol, M. WW domain. In: Cesareni, GGM.; Sudol, M.; Yaffe, M., editors. Modular Protein Domains. Wiley VCH, Verlag GmbH & Co; Weinheim, Germany: 2004. p. 59-72.
43. McDonald CB, Buffa L, Bar-Mag T, Salah Z, Bhat V, Mikles DC, Deegan BJ, Seldeen KL, Malhotra A, Sudol M, Aqeilan RI, Nawaz Z, Farooq A. Biophysical basis of the binding of WWOX tumor suppressor to WBP1 and WBP2 adaptors. J Mol Biol. 2012; 422:58–74. [PubMed: 22634283]
44. Gao X, Yo P, Keith A, Ragan TJ, Harris TK. Thermodynamically balanced inside-out (TBIO) PCR-based gene synthesis: a novel method of primer design for high-fidelity assembly of longer gene sequences. Nucleic Acids Res. 2003; 31:e143. [PubMed: 14602936]
45. Gasteiger, E.; Hoogland, C.; Gattiker, A.; Duvaud, S.; Wilkins, MR.; Appel, RD.; Bairoch, A. Protein Identification and Analysis Tools on the ExPASy Server. In: Walker, JM., editor. The Proteomics Protocols Handbook. Humana Press; Totowa, New Jersey, USA: 2005. p. 571-607.
46. Wiseman T, Williston S, Brandts JF, Lin LN. Rapid measurement of binding constants and heats of binding using a new titration calorimeter. Anal Biochem. 1989; 179:131–137. [PubMed: 2757186]
47. Zimm BH. The Scattering of Light and the Radial Distribution Function of High Polymer Solutions. J Chem Phys. 1948; 16:1093–1099.
48. Wyatt PJ. Light Scattering and the Absolute Characterization of Macromolecules. Anal Chim Acta. 1993; 272:1–40.
49. Berne, BJ.; Pecora, R. Dynamic Light Scattering. Wiley; New York: 1976.
50. Chu, B. Laser Light Scattering: Basic Principles and Practice. Academic; Boston, Massachusetts: 1991.
51. Koppel DE. Analysis of Macromolecular Polydispersity in Intensity Correlation Spectroscopy. J Chem Phys. 1972; 57:4814–4820.
52. Marti-Renom MA, Stuart AC, Fiser A, Sanchez R, Melo F, Sali A. Comparative Protein Structure Modeling of Genes and Genomes. Annu Rev Biophys Biomol Struct. 2000; 29:291–325. [PubMed: 10940251]
53. Carson M. Ribbons 2.0. J Appl Crystallogr. 1991; 24:958–961.
54. Van Der Spoel D, Lindahl E, Hess B, Groenhof G, Mark AE, Berendsen HJ. GROMACS: fast, flexible, and free. J Comput Chem. 2005; 26:1701–1718. [PubMed: 16211538]
55. Lindorff-Larsen K, Piana S, Palmo K, Maragakis P, Klepeis JL, Dror RO, Shaw DE. Improved side-chain torsion potentials for the Amber ff99SB protein force field. Proteins. 2010; 78:1950–1958. [PubMed: 20408171]
56. Toukan K, Rahman A. Molecular-dynamics study of atomic motions in water. Physical Review B. 1985; 31:2643–2648.
57. Darden TA, York D, Pedersen L. Particle mesh Ewald: An N.log(N) method for Ewald sums in large systems. J Chem Phys. 1993; 98:10089–10092.
58. Hess B, Bekker H, Berendsen HJC, Fraaije JGEM. LINCS: A linear constraint solver for molecular simulations. J Comput Chem. 1997; 18:1463–1472.
59. Macias MJ, Hyvonen M, Baraldi E, Schultz J, Sudol M, Saraste M, Oschkinat H. Structure of the WW domain of a kinase-associated protein complexed with a proline-rich peptide. Nature. 1996; 382:646–649. [PubMed: 8757138]

60. Pires JR, Taha-Nejad F, Toepert F, Ast T, Hoffmuller U, Schneider-Mergener J, Kuhne R, Macias MJ, Oschkinat H. Solution structures of the YAP65 WW domain and the variant L30 K in complex with the peptides GTPPPPYTVG, N-(n-octyl)-GPPPY and PLPPY and the application of peptide libraries reveal a minimal binding epitope. J Mol Biol. 2001; 314:1147–1156. [PubMed: 11743730]
61. Huang X, Poy F, Zhang R, Joachimiak A, Sudol M, Eck MJ. Structure of a WW domain containing fragment of dystrophin in complex with beta-dystroglycan. Nat Struct Biol. 2000; 7:634–638. [PubMed: 10932245]
62. Kanelis V, Rotin D, Forman-Kay JD. Solution structure of a Nedd4 WW domain-ENaC peptide complex. Nat Struct Biol. 2001; 8:407–412. [PubMed: 11323714]
63. Palencia A, Camara-Artigas A, Pisabarro MT, Martinez JC, Luque I. Role of interfacial water molecules in proline-rich ligand recognition by the Src homology 3 domain of Abl. J Biol Chem. 2010; 285:2823–2833. [PubMed: 19906645]
64. Martin-Garcia JM, Ruiz-Sanz J, Luque I. Interfacial water molecules in SH3 interactions: a revised paradigm for polyproline recognition. Biochem J. 2012; 442:443–451. [PubMed: 22115123]
65. Zafra-Ruano A, Luque I. Interfacial water molecules in SH3 interactions: Getting the full picture on polyproline recognition by protein-protein interaction domains. FEBS Lett. 2012; 586:2619–2630. [PubMed: 22584053]
66. Ohnishi S, Guntert P, Koshiba S, Tomizawa T, Akasaka R, Tochio N, Sato M, Inoue M, Harada T, Watanabe S, Tanaka A, Shirouzu M, Kigawa T, Yokoyama S. Solution structure of an atypical WW domain in a novel beta-clam-like dimeric form. FEBS Lett. 2007; 581:462–468. [PubMed: 17239860]
67. Huang X, Beullens M, Zhang J, Zhou Y, Nicolaescu E, Lesage B, Hu Q, Wu J, Bollen M, Shi Y. Structure and function of the two tandem WW domains of the pre-mRNA splicing factor FBP21 (formin-binding protein 21). J Biol Chem. 2009; 284:25375–25387. [PubMed: 19592703]
68. Nimnual A, Bar-Sagi D. The two hats of SOS. Sci STKE. 2002; 2002:PE36. [PubMed: 12177507]
69. Pierre S, Bats AS, Coumoul X. Understanding SOS (Son of Sevenless). Biochem Pharmacol. 2011; 82:1049–1056. [PubMed: 21787760]
70. Li N, Batzer A, Daly R, Yajnik V, Skolnik E, Chardin P, Bar-Sagi D, Margolis B, Schlessinger J. Guanine-nucleotide-releasing factor hSos1 binds to Grb2 and links receptor tyrosine kinases to Ras signalling. Nature. 1993; 363:85–88. [PubMed: 8479541]
71. Rozakis-Adcock M, Fernley R, Wade J, Pawson T, Bowtell D. The SH2 and SH3 domains of mammalian Grb2 couple the EGF receptor to the Ras activator mSos1. Nature. 1993; 363:83–85. [PubMed: 8479540]
72. Chardin P, Camonis JH, Gale NW, van Aelst L, Schlessinger J, Wigler MH, Bar-Sagi D. Human Sos1: a guanine nucleotide exchange factor for Ras that binds to GRB2. Science. 1993; 260:1338–1343. [PubMed: 8493579]
73. Nimnual AS, Yatsula BA, Bar-Sagi D. Coupling of Ras and Rac guanosine triphosphatases through the Ras exchanger Sos. Science. 1998; 279:560–563. [PubMed: 9438849]
74. Innocenti M, Tenca P, Frittoli E, Faretta M, Tocchetti A, Di Fiore PP, Scita G. Mechanisms through which Sos-1 coordinates the activation of Ras and Rac. J Cell Biol. 2002; 156:125–136. [PubMed: 11777939]
75. Reuther GW, Der CJ. The Ras branch of small GTPases: Ras family members don't fall far from the tree. Curr Opin Cell Biol. 2000; 12:157–165. [PubMed: 10712923]
76. Robinson MJ, Cobb MH. Mitogen-activated protein kinase pathways. Curr Opin Cell Biol. 1997; 9:180–186. [PubMed: 9069255]
77. Hall A. Rho GTPases and the actin cytoskeleton. Science. 1998; 279:509–514. [PubMed: 9438836]
78. Ridley AJ. Rho GTPases and cell migration. J Cell Sci. 2001; 114:2713–2722. [PubMed: 11683406]
79. Sundvall M, Korhonen A, Paatero I, Gaudio E, Melino G, Croce CM, Aqeilan RI, Elenius K. Isoform-specific monoubiquitination, endocytosis, and degradation of alternatively spliced ErbB4 isoforms. Proc Natl Acad Sci U S A. 2008; 105:4162–4167. [PubMed: 18334649]

80. Li Y, Zhou Z, Alimandi M, Chen C. WW domain containing E3 ubiquitin protein ligase 1 targets the full-length ErbB4 for ubiquitin-mediated degradation in breast cancer. Oncogene. 2009; 28:2948–2958. [PubMed: 19561640]

81. Feng SM, Muraoka-Cook RS, Hunter D, Sandahl MA, Caskey LS, Miyazawa K, Atfi A, Earp HS 3rd. The E3 ubiquitin ligase WWP1 selectively targets HER4 and its proteolytically derived signaling isoforms for degradation. Mol Cell Biol. 2009; 29:892–906. [PubMed: 19047365]

82. Zeng F, Xu J, Harris RC. Nedd4 mediates ErbB4 JM-a/CYT-1 ICD ubiquitination and degradation in MDCK II cells. FASEB J. 2009; 23:1935–1945. [PubMed: 19193720]

83. Fedoroff OY, Townson SA, Golovanov AP, Baron M, Avis JM. The Structure and Dynamics of Tandem WW Domains in a Negative Regulator of Notch Signaling, Suppressor of Deltex. J Biol Chem. 2004; 279:34991–35000. [PubMed: 15173166]

84. Wiesner S, Stier G, Sattler M, Macias MJ. Solution Structure and Ligad Recognition of the WW Domain of the Yeast Splicing Factor Prp40. J Mol Biol. 2002; 324:807–822. [PubMed: 12460579]

85. Patnaik A, Wills JW. In vivo interference of Rous sarcoma virus budding by cis expression of a WW domain. J Virol. 2002; 76:2789–2795. [PubMed: 11861846]

86. Sudol M, Harvey KF. Modularity in the Hippo signaling pathway. Trends Biochem Sci. 2010; 35:627–633. [PubMed: 20598891]

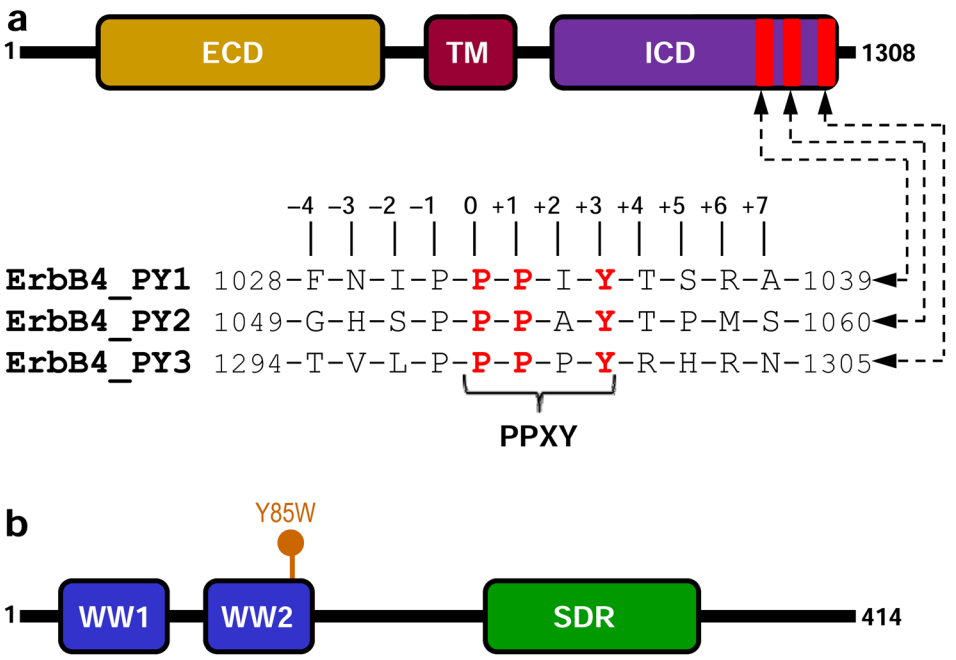

Figure 1.

Modular organization of human ErbB4 and WWOX proteins. (a) ErbB4 contains the canonical ECD-TM-ICD receptor tyrosine kinase modular cassette, where the central single-helical transmembrane (TM) domain is flanked between an N-terminal extracellular (ECD) and a C-terminal intracellular (ICD) domains. The three PPXY motifs (designated PY1, PY2 and PY3) within the ICD are located at the extreme C-terminus. Note that the amino acid sequence of 12-mer peptides containing the PPXY motifs and flanking residues are provided. The numerals indicate the nomenclature used in this study to distinguish residues within and flanking the motifs relative to the first proline within the PPXY motifs, which is arbitrarily assigned zero. (b) WWOX is comprised of a tandem copy of WW domains, designated WW1 and WW2, located N-terminal to the short-chain dehydrogenase/reductase (SDR) domain. The location of Y85W mutation within the WW2 domain is indicated.

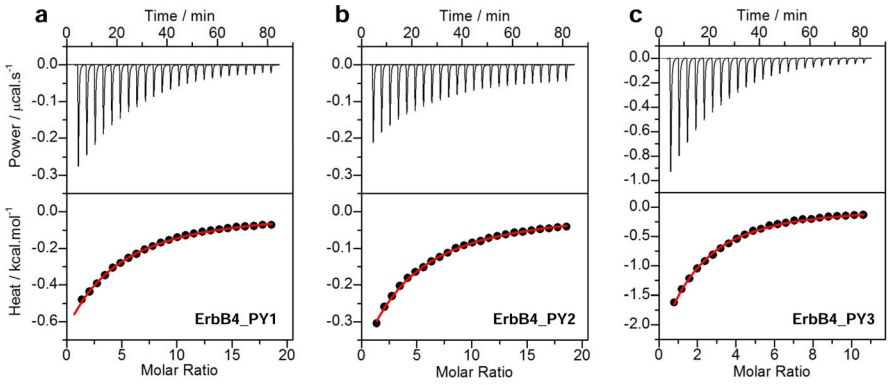

Figure 2.

ITC analysis for the binding of WW1 domain of WWOX to ErbB4_PY1 (a), ErbB4_PY2 (b) and ErbB4_PY3 (c) peptides. The upper panels show the raw ITC data expressed as change in thermal power with respect to time over the period of titration. In the lower panels, change in molar heat is expressed as a function of molar ratio of corresponding peptide to WW1 domain. The red solid lines in the lower panels show the fit of data to a one-site binding model using the integrated ORIGIN software as described earlier (43, 46).

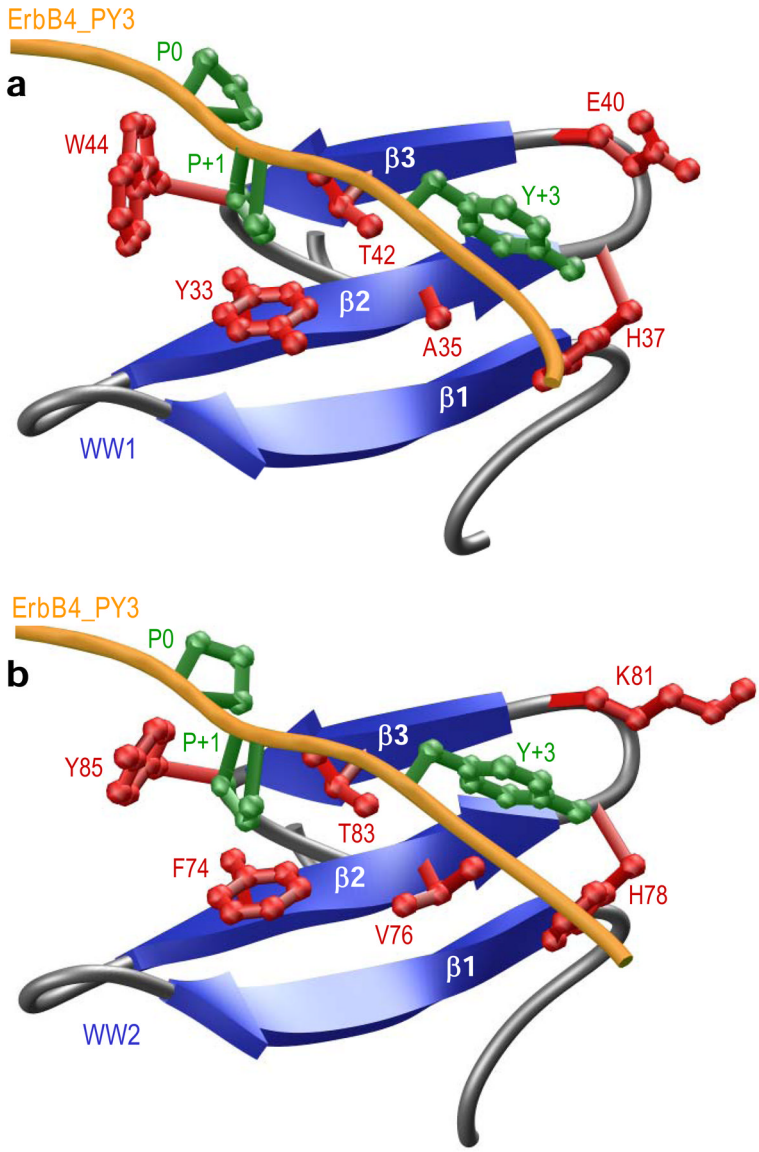

Figure 3.

Structural models of WW1 (a) and WW2 (b) domains of WWOX in complex with ErbB4_PY3 peptide containing the PPXY motif. In each case, the β-strands within the WW domain are shown in blue with loops depicted in gray and the PPXY peptide is colored yellow. The sidechain moities of residues within the WW domain and the PPXY peptide engaged in key intermolecular contacts are shown in red and green, respectively. Note that the first two N-terminal proline residues within the PPXY motif are respectively P0 and P +1, while the C-terminal Y is indicated by Y+3.

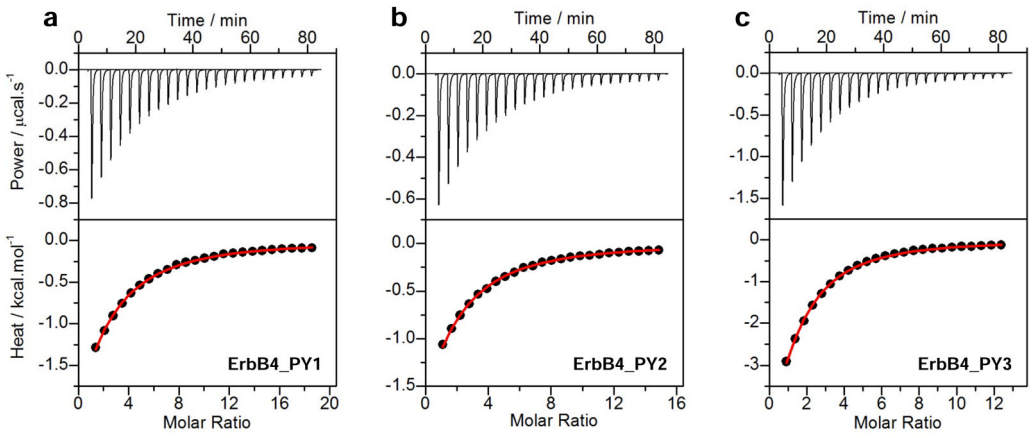

Figure 4.

ITC analysis for the binding of WW1–WW2 tandem module of WWOX to ErbB4_PY1 (a), ErbB4_PY2 (b) and ErbB4_PY3 (c) peptides. The upper panels show the raw ITC data expressed as change in thermal power with respect to time over the period of titration. In the lower panels, change in molar heat is expressed as a function of molar ratio of corresponding peptide to WW1–WW2 tandem module. The red solid lines in the lower panels show the fit of data to a one-site binding model using the integrated ORIGIN software as described earlier (43, 46).

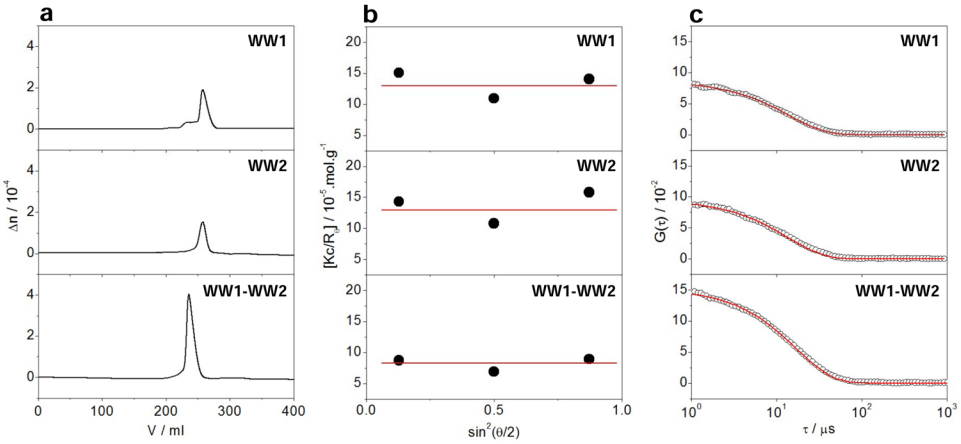

Figure 5.

ALS analysis of WW1 (top panels) and WW2 (middle panels) domains alone and in the context of WW1–WW2 tandem module (bottom panels) of WWOX. (a) Elution profiles as monitored by the differential refractive index (Δn) of each protein construct plotted as a function of elution volume (V). (b) Partial Zimm plots obtained for each protein construct from analytical SLS measurements. Note that the red solid lines through the data points represent linear fits. (c) Autocorrelation function plots obtained for each protein construct from analytical DLS measurements. Note that the red solid lines represent non-linear least squares fit of data to an autocorrelation function as embodied in Eq [9].

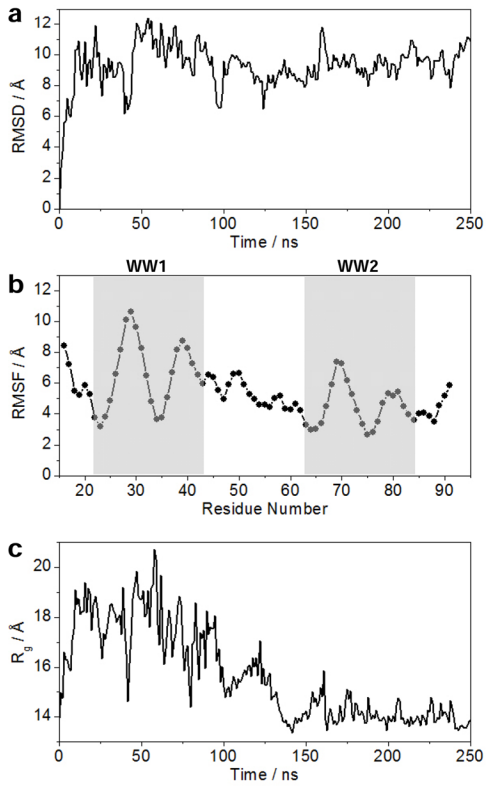

Figure 6.

MD analysis conducted on the structural model of WW1–WW2 tandem module of WWOX. (a) Root mean square deviation (RMSD) of backbone atoms (N, Cα and C) within each simulated structure relative to the initial modeled structure as a function of simulation time. (b) Root mean square fluctuation (RMSF) of backbone atoms (N, Cα and C) averaged over the entire course of MD trajectory as a function of residue number. The vertical boxes demarcate the boundaries of WW1 and WW2 domains. (c) Radius of gyration (R_g) of each simulated structure relative to the initial modeled structure as a function of simulation time.

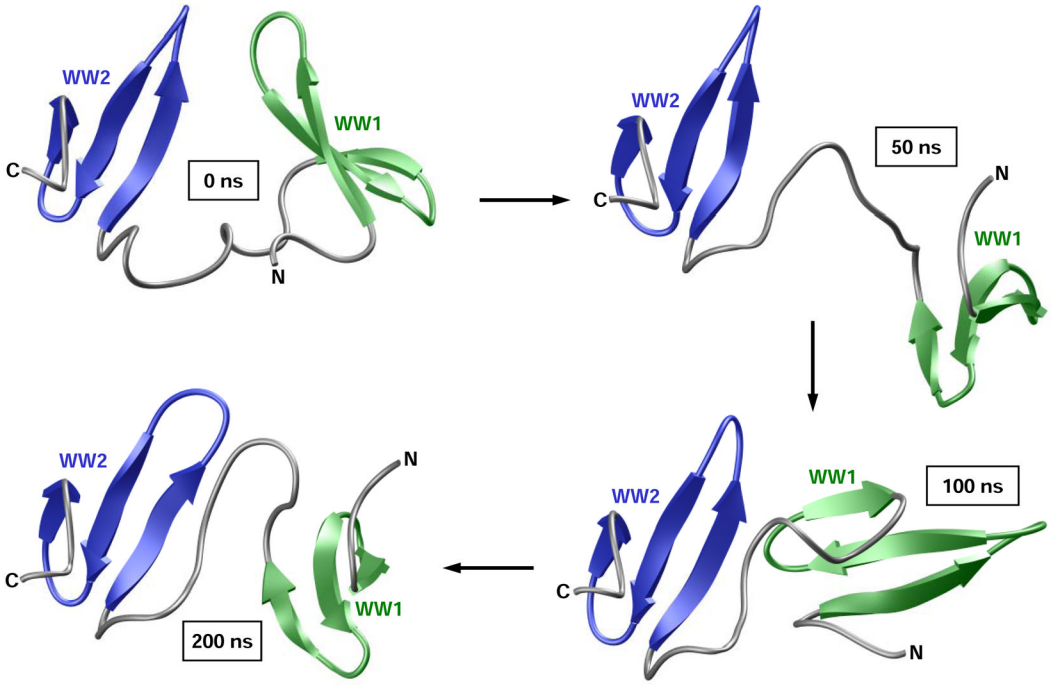

Figure 7.

Structural snapshots taken at 0ns, 50ns, 100ns and 200ns during the course of an MD simulation conducted on the structural model of WW1–WW2 tandem module of WWOX. The constituent WW1 and WW2 domains are respectively colored green and blue, while the terminal and interdomain loops are shown in gray for clarity.

Table 1

Thermodynamic parameters for the binding of WW1 domain of WWOX to PPXY peptides derived from the ICD of ErbB4

Peptide	Sequence	K_d/μM	ΔH/kcal.mol^{-1}	TΔS/kcal.mol^{-1}	ΔG/kcal.mol^{-1}
ErbB4_PY1	FNIP**PP**I**Y**TSRA	383 ± 30	−6.88 ± 0.48	−2.21 ± 0.43	−4.67 ± 0.05
ErbB4_PY2	GHSP**PP**A**Y**TPMS	362 ± 45	−3.66 ± 0.33	+1.04 ± 0.40	−4.70 ± 0.07
ErbB4_PY3	TVLP**PP**P**Y**RHRN	144 ± 16	−6.21 ± 0.54	−1.24 ± 0.10	−5.25 ± 0.06

All parameters were obtained from ITC measurements at pH 7.0 and 25°C. Note that the consensus residues within the PPXY motif of each peptide are colored blue for clarity. All binding stoichiometries were fixed to unity. Errors were calculated from at least three independent measurements. All errors are given to one standard deviation.

Table 2

Thermodynamic parameters for the binding of WW1 domain of WWOX to wildtype (PY3_WT) and single alanine mutants of ErbB4_PY3 peptide

Peptide	Sequence	K_d/μM	ΔH/kcal.mol^{-1}	TΔS/kcal.mol^{-1}	ΔG/kcal.mol^{-1}
PY3_WT	TVLPPPPYRHRN	144 ± 16	−6.21 ± 0.54	−1.24 ± 0.10	−5.25 ± 0.06
PY3_A−3	TALPPPPYRHRN	113 ± 21	−3.67 ± 0.23	+1.73 ± 0.34	−5.40 ± 0.11
PY3_A−2	TVAPPPPYRHRN	151 ± 15	−6.19 ± 0.60	−1.32 ± 1.16	−5.22 ± 0.07
PY3_A−1	TVLAPPPYRHRN	161 ± 29	−3.33 ± 0.42	+1.86 ± 0.52	−5.19 ± 0.11
PY3_A0	TVLPAPPYRHRN	NBD	NBD	NBD	NBD
PY3_A+1	TVLPPAPYRHRN	NBD	NBD	NBD	NBD
PY3_A+2	TVLPPPAYRHRN	287 ± 37	−3.63 ± 0.30	+1.21 ± 0.37	−4.84 ± 0.08
PY3_A+3	TVLPPPPARHRN	NBD	NBD	NBD	NBD
PY3_A+4	TVLPPPPYAHRN	275 ± 64	−4.02 ± 0.24	+0.85 ± 0.38	−4.87 ± 0.14
PY3_A+5	TVLPPPPYRARN	157 ± 18	−11.40 ± 1.41	−6.20 ± 1.48	−5.20 ± 0.07
PY3_A+6	TVLPPPPYRHAN	135 ± 30	−4.78 ± 0.26	+0.52 ± 0.39	−5.29 ± 0.13

All parameters were obtained from ITC measurements at pH 7.0 and 25°C. Note that the alanine substitutions within the ErbB4_PY3 peptide are colored red and underlined, whilst the consensus residues within the PPXY motif are colored blue for clarity. All binding stoichiometries were fixed to unity. Errors were calculated from at least three independent measurements. All errors are given to one standard deviation. NBD indicates no binding determined due to weak interactions (K_d > 1mM).

Table 3

Thermodynamic parameters for the binding of WW2W domain of WWOX to PPXY peptides derived from the ICD of ErbB4

Peptide	Sequence	K_d/μM	ΔH/kcal.mol^{-1}	TΔS/kcal.mol^{-1}	ΔG/kcal.mol^{-1}
ErbB4_PY1	FNIP**PP**I**Y**TSRA	680 ± 121	−4.74 ± 0.52	−0.40 ± 0.62	−4.33 ± 0.11
ErbB4_PY2	GHSP**PP**A**Y**TPMS	620 ± 55	−8.08 ± 1.09	−3.70 ± 1.14	−4.38 ± 0.05
ErbB4_PY3	TVLP**PP**P**Y**RHRN	54 ± 9	−4.15 ± 0.28	+1.68 ± 0.37	−5.83 ± 0.09

All parameters were obtained from ITC measurements at pH 7.0 and 25°C. Note that the WW2W domain is the mutant construct of WW2 domain harboring the Y85W substitution. The consensus residues within the PPXY motif of each peptide are colored blue for clarity. All binding stoichiometries were fixed to unity. Errors were calculated from at least three independent measurements. All errors are given to one standard deviation. NBD indicates no binding determined due to weak interactions (K_d > 1mM).

Table 4

Thermodynamic parameters for the binding of WW1–WW2 tandem module of WWOX to PPXY peptides derived from the ICD of ErbB4

Peptide	Sequence	K_d/μM	ΔH/kcal.mol^{-1}	TΔS/kcal.mol^{-1}	ΔG/kcal.mol^{-1}
ErbB4_PY1	FNIP**PP**I**Y**TSRA	170 ± 12	−7.25 ± 0.88	−2.10 ± 0.92	−5.15 ± 0.04
ErbB4_PY2	GHSP**PP**A**Y**TPMS	175 ± 13	−4.88 ± 0.28	+0.26 ± 0.34	−5.13 ± 0.05
ErbB4_PY3	TVLP**PP**P**Y**RHRN	68 ± 8	−5.00 ± 0.30	+0.70 ± 0.37	−5.70 ± 0.07

All parameters were obtained from ITC measurements at pH 7.0 and 25°C. Note that the consensus residues within the PPXY motif of each peptide are colored blue for clarity. All binding stoichiometries were fixed to unity. Errors were calculated from at least three independent measurements. All errors are given to one standard deviation.

Table 5

Hydrodynamic parameters for WW domains alone and in the context of WW1–WW2 tandem module of WWOX

Construct	M_w/kD	M_n/kD	M_w/M_n	R_h/Å	Associativity
WW1	9 ± 2	9 ± 1	1.06 ± 0.08	18 ± 1	Monomer
WW2	10 ± 1	9 ± 1	1.02 ± 0.03	19 ± 1	Monomer
WW1–WW2	14 ± 1	14 ± 1	1.03 ± 0.04	27 ± 1	Monomer

All parameters were obtained from ALS measurements at pH 7.0 and 25°C. Note that the calculated molar masses of recombinant WW1, WW2 and WW1–WW2 constructs from their respective amino acid sequence are 9kD, 9kD and 14kD, respectively. Errors were calculated from at least three independent measurements. All errors are given to one standard deviation.